Investigation on plasma structure evolution and discharge characteristics of a single-stage planar-pulsed-inductive accelerator under ambient fill condition*

Xiao-Kang Li(李小康), Bi-Xuan Che(车碧轩)†, Mou-Sen Cheng(程谋森), Da-Wei Guo(郭大伟), Mo-Ge Wang(王墨戈), and Yun-Tian Yang(杨云天)

College of Aerospace Science and Engineering, National University of Defense Technology, Changsha 410073, *China*

(Received 15 May 2020; revised manuscript received 9 June 2020; accepted manuscript online 23 June 2020)

The physical process of a single-stage planar-pulsed-inductive accelerator is investigated. Measurements include the waveforms of circuit current, capacitor voltage, plasma radiation intensity, and temporal plasma structure photos captured by a high-speed camera. Experiments are conducted under static ambient fill condition using argon as propellant. Varied values of capacitor voltage and gas pressure are compared. Further discussions quantify the EM interaction between circuit and plasma, as well as their energy deposition and current sheet acceleration. Based on the results of experiments, physical mechanisms of the initial ionization phase and the following acceleration phase are analyzed theoretically.

Keywords: electric propulsion, pulsed-inductive thruster, discharge characteristics, plasma structure

PACS: 52.77.–j, 52.75.Di, 52.80.–s, 84.30.Ng **DOI:** 10.1088/1674-1056/ab9f2a

1. Introduction

Pulsed-inductive thruster (PIT), also known as inductive-pulsed plasma thruster (IPPT), is a sort of plasma accelerator used in in-space propulsion, which impulsively and inductively expels a toroidal plasma current sheet through the pulsed electromagnetic (EM) field induced by a planar annular drive-coil. Because of its inductive nature, PIT suffers less from electrode-erosion-related lifetime, contamination or multi-propellant feasibility problems compared with common ion or Hall thrusters. These advantages make PIT one of the most promising candidates for future high-power electric propulsion (EP) systems.[1,2]

Researches and developments of PITs have continued more than 50 years, while no propulsion system has been deployed in orbit till now. The immatureness is caused by many reasons: the lack of competent components (switch, capacitor and valve), the ever-weak demand for high power EP systems in the 1990s, and more essentially, the relatively poor understanding of its inherent physics.[3]

In some devices the circular electric field that arises from the time-varying magnetic field ionizes the propellant,[4,5] while in other devices, the propellant is ionized separately employing glow electrodes or radio frequency antenna.[6,7] Owing to the system simplicity and reliability, the former single-stage devices keep the mainstream of PIT development. Two inherent physical effects dominate the performance of such single-stage PITs: the ionization process at the beginning phase of each pulse and the acceleration process during the main period.

Very few researches considered the initial ionization process, about which merely an empirical condition for the drive-coil current density rise rate was proposed by Polzin.[8] Studies around the acceleration process mainly focused on the structure of plasma current sheet, about which probes such as B-dot probe, micro Rogowsky coil, and Langmuir probe were respectively used to measure the EM field intensity, current density, and plasma parameters at limited points.[9–11] The results confirmed that, screening the magnetic field of drive-coil under plasma current sheet can enhance the coupling between plasma and circuit, and consequently improve the thruster performance. Besides, the relative time scale of plasma movement and circuit current waveform also influences the acceleration effect, where an optimum dynamic impedance condition is required to be matched. This phenomenon was primarily studied by direct thrust impulse measurements[3] and numerical simulations employing slug models[12,13] or MHD models.[14–16]

In this paper, a 1000-J level pulsed-inductive accelerator is constructed to reproduce the working process of PITs. The plasma structure evolution is studied adopting a high-speed camera in correlation with discharge characteristics including circuit current, capacitor voltage, and plasma radiation intensity. To exclude the influence of initial gas nonuniformity, experiments are conducted under static ambient fill condition. The propellant used is argon. Based on the results of experiments, the physical mechanisms of both ionization process and acceleration process are analyzed.

*Project supported by the Hunan Provincial Natural Science Foundation of China (Grant No. 2018JJ3592).

†Corresponding author. E-mail: chebixuan@outlook.com

© 2020 Chinese Physical Society and IOP Publishing Ltd

2. Experiment setup

Figure 1 presents the schematic diagram of experiment setup, which consists of a pulse-forming network (PFN), a gas delivery apparatus, a transparent discharge chamber, as well as the supporting diagnostic, data acquisition, and control subsystems.

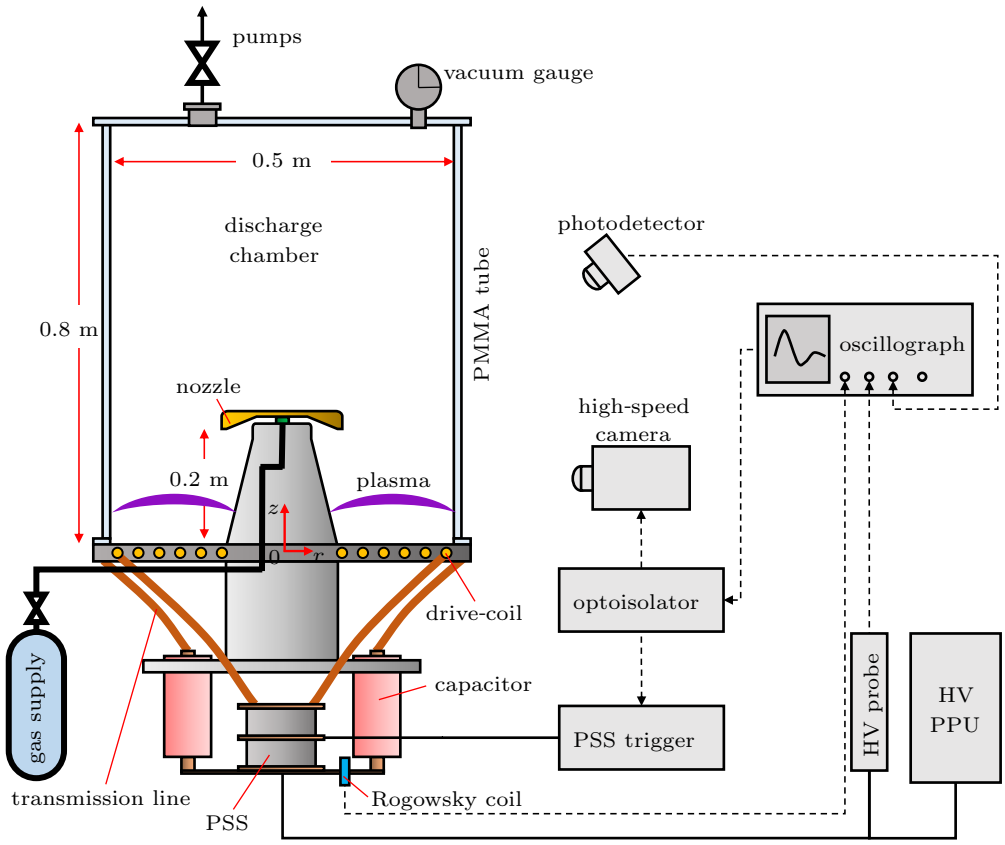


Fig. 1. Schematic diagram of experiment setups.

As shown in Fig. 2, the accelerator is equipped with a 0.5-m diameter drive-coil with 16 pieces of one-turn spiral conductor arranged axisymmetrically. The conductors are packaged in an epoxy resin plate to avoid direct contact with plasma. The pulse energy is initially stored in eight high-voltage thin-film capacitors and then released under the control of a pseudo-spark switch (PSS). The capacitors are placed axisymmetrically around the PSS to guarantee discharge synchronization (Fig. 4), and then each connected to two pieces of drive-coil conductor to make sure the current density distribution identical (Fig. 3). The capacitors, drive-coil and PSS form an RLC-type PFN, whose circuit parameters are presented in Table 1.

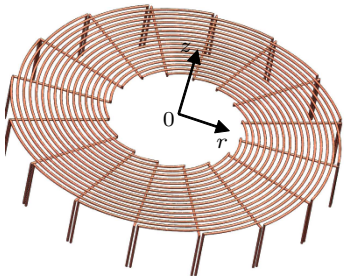


Fig. 2. Configuration of drive-coil.

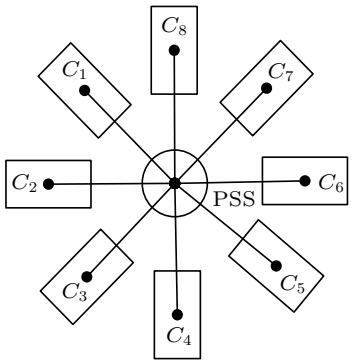


Fig. 3. Arrange of capacitors.

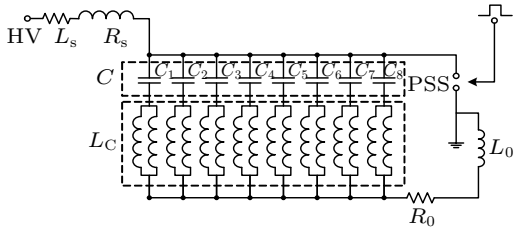


Fig. 4. Circuit schematic diagram of pulse-forming network (PFN).

A polymethylmethacrylate (PMMA) tube is mounted onto the front face of drive-coil plate, forming a discharge chamber where the plasma is induced and accelerated. On a

practical PIT, propellant is injected by a pulsed gas injector which equips a high-speed valve.[17] However, in this preliminary study, the propellant is feed through a hand valve successively. By pumping out the gas in the chamber and refills it with argon, a static ambient fill condition is achieved. The gas pressure p_0 is measured by a capacitance diaphragm vacuum gauge (CERAVAC CTR101N).

Table 1. Circuit parameters of pulse-forming network.

Drive-coil inductance	Total capacitance	Parasitic resistance	Parasitic inductance
L_C/nH	C/μF	R_0/mΩ	L_0/nH
378	8	13	123

High-speed photographing is a potent way to study plasma flow processes.[18] A high-speed camera (FASTCAM SA-Z) is adopted to observe the plasma structure from side view through the transparent chamber wall. The exposure time is fixed at 0.95 μs. The circuit current I_C and capacitor voltage V are monitored by a Rogowsky coil (Pearson 5046) and an HV probe (Tektronix P6015A) respectively. The radiation intensity of plasma U_R is detected by a photodetector (Thorlabs DET 10A). When the capacitor bank is charged to a given voltage V_0, the oscillograph controls the PSS trigger to switch on the PSS and at the same time ignites the high-speed camera. An optoisolator is used to protect the oscillograph from electric overshooting as well as to improve the synchronicity of high-speed camera.

3. Results and discussion

Three V_0 values (8.4, 13.2, and 17.2 kV) and four p_0 values (80, 50, 20, and 10 Pa) are compared in twelve cases. For each case, at least three repeated shots are performed and as a result, good repeatability of phenomena is demonstrated. A bright plasma loop (as shown in Fig. 5) is generated in all the shots, but notable axial acceleration of plasma can only be observed under higher V_0 and lower p_0. This fact implies that the effective acceleration of plasma requires higher than merely ionizing the propellant. Four cases ($V_0 = 8.4$, 17.2 kV and $p_0 = 50$, 10 Pa) clearly exhibit the typical features and variation trends of phenomena. Their high-speed camera frames as well as discharge waveforms are explored in this section to gain insights into the underlying physical process. Further, three derived parameters including the Lovberg ratio L^*, the plasma energy deposition ratio ε, and the exhausting speed v_t are calculated based on the experimental results. These parameters are used to quantify the EM coupling strength, the energy deposition efficiency, and the acceleration performance of different cases respectively.

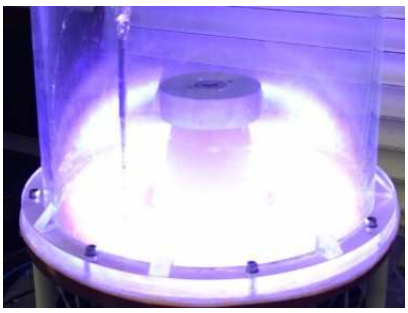


Fig. 5. Long exposure photograph of the discharge process.

3.1. Discharge process

Representative frames of the four typical cases are provided in Fig. 6, while the corresponding waveforms of I_C, V, and U_R are shown in Figs. 7–9.

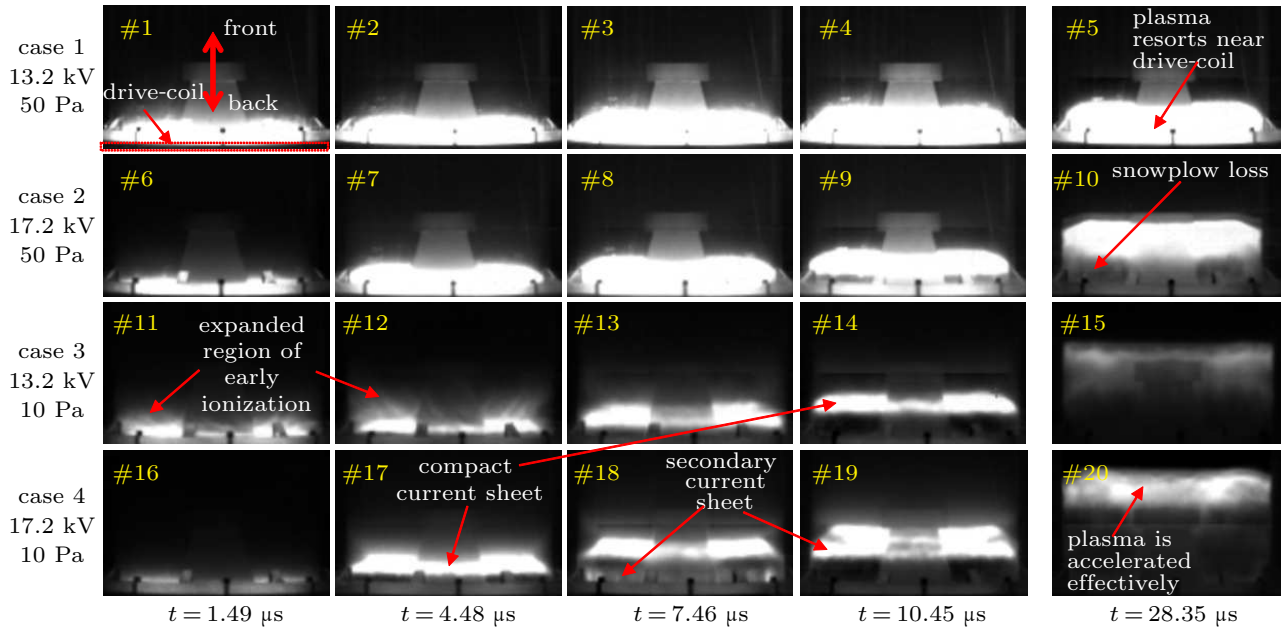


Fig. 6. Representative frames of high speed photographing.

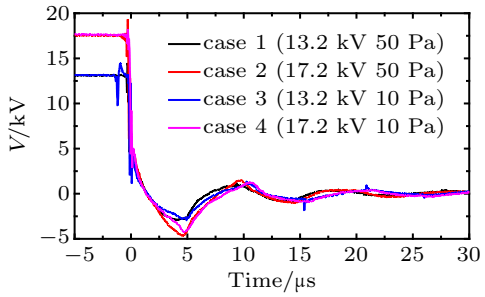


Fig. 7. Capacitor voltage V.

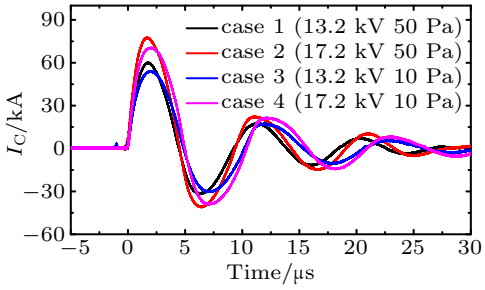


Fig. 8. Circuit current I_C.

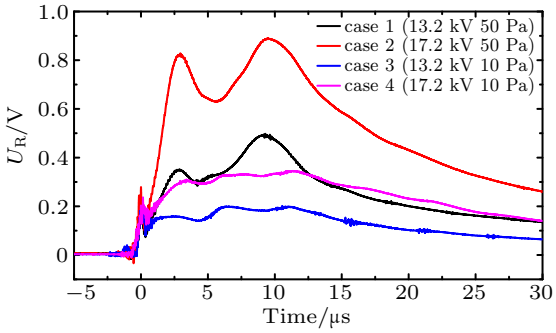


Fig. 9. Plasma radiation intensity U_R.

In case 1, the toroidal plasma current sheet seems to resort near the drive-coil surface during the whole pulse period. Even at $t = 28.35$ μs when I_C almost attenuates to zero, little effective acceleration can be distinguished (#5). The fluctuation of U_R homologous with I_C also demonstrate a strong coupling relationship between plasma and circuit, suggesting that the separation distance between them is not far.

In case 2, V_0 is increased over case 1. A detachment between current sheet back edge and drive-coil surface can be seen at $t = 10.45$ μs (#9), indicating that the Lorentz force has overcome the gas dynamic force and successfully driven the current sheet away. At $t = 28.35$ μs (#10), an expanded tail of plasma can be found, which was known as "snowplow loss" in literature,[3] indicating that part of the current sheet mass is dragged back or left behind. The U_R curve of case 2 is much higher than the others and its fluctuation is also apparent, indicating a notable radiative loss of energy and a strong coupling between circuit and plasma.

In case 3, p_0 is lower than that in case 1 while their V_0 values are identical. Different phenomena are observed at both ionization and acceleration phase. At $t = 1.49$ μs, the ionized region is more expanded and ununiform in case 3 (#11) than in case 1 (#1). The crown-like plasma branches on the front edge of current sheet keep growing at $t = 4.48$ μs (#12), but soon shrink back at $t = 7.46$ μs (#13). Then a flat and compact current sheet is observed (#14), which keeps its shape for a long period until I_C approaches zero at $t = 28.35$ μs (#15). The back region of this current sheet is also more clear and darker, indicating less snowplow loss. The U_R curve of case 3 experiences a relatively smooth period from about $t = 2$ μs to 12 μs, which is probably caused by a combined action of current sheet departure and circuit current growth.

In case 4, V_0 is increased over case 3. It should be noticed that the region of ionization at early time is the smallest and no crown-like plasma branches can be seen in this case (#16). Then at $t = 4.48$ μs (#17), a flat and compact current sheet with clear detachment from drive-coil surface is observed. This current sheet moves fast in the four discussed cases and its snowplow loss is also neglectable. It is interesting to find that, a secondary current sheet is induced at $t = 7.46$ μs (#18), when the corresponding I_C curve arrives its negative maximum. This secondary current sheet soon catches up the primary current sheet at $t = 10.45$ μs (#19) and then integrates with it. Similar smooth trend of U_R like case 3 can also be seen in this case.

3.2. Derived parameters

The PFN and plasma can be respectively treated as the primary and secondary stage of a transformer as shown in Fig. 10, where the mutual inductance M between drive-coil and current sheet is strongly determined by their separation distance z.

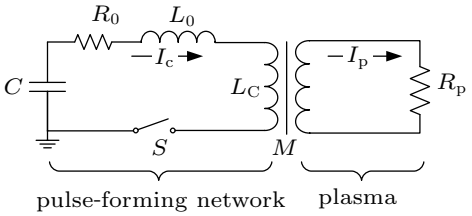


Fig. 10. Lumped elementary circuit model of a pulsed-inductive accelerator.

Replacing the current sheet with a metal annulus, Dailey's measurements has found that the total inductance L_t can be very closely approximated by the exponential function[4]

$$L_t(z) = L_0 + L_C \exp(1 - z/z_0), \tag{1}$$

where z_0 was defined as the decoupling stroke length of drive-coil. Adopting the same method as Dailey, z_0 is measured to be 5 cm for the drive-coil in this study. The metal nozzle of gas injector is mounted at $z = 4z_0$, where the effect of drive-coil field can be ignored. Then, the exhausting speed v_t is de-

fined as the average velocity of current sheet front edge from $t = 0$ μs to the time when it arrives at the nozzle.

L_t may drop suddenly at the beginning of each pulse because of gas breakdown, after that increases with the movement of current sheet, and then probably drops again when the secondary current sheet emerges. Besides z, M is also determined by the structure and conductivity of current sheet. Ignoring these time variations, the average total inductance $\bar{L}_t$ is estimated by curve-fitting of I_C traces using MATLAB curve-fitting tool based on the theoretic LCR equation:[19]

$$I_C(t) = \frac{V_0}{\sqrt{1-\xi^2}}\sqrt{\frac{C}{\bar{L}_t}}\,e^{-\xi(t/\sqrt{\bar{L}_t C})}\sin\left(t\sqrt{\frac{1-\xi^2}{\bar{L}_t C}}\right),$$
$$\xi = \frac{\bar{R}_t}{2\sqrt{\bar{L}_t/C}}. \quad (2)$$

After that, the Lovberg ratio L^*[20] is modified here to compare the global EM coupling strength between PFN and plasma:

$$L^* = \frac{L_C + L_0 - \bar{L}_t}{L_C + L_0}. \quad (3)$$

According to its definition, L^* essentially quantifies the average fraction of drive-coil magnetic flux that couples with plasma during the pulse period.

During the discharge period, the pulse energy initially stored in the capacitors keeps coupling into plasma and dissipating through the parasitic resistance R_0 of PFN. The energy has deposited into plasma then becomes its internal energy (thermal and ionization), or dissipates through plasma radiation, or converses into propulsive macroscopic axial kinetic energy. Indiscriminating these different energy forms in plasma, the total energy that has deposited into plasma can be simply computed by subtracting the cumulate resistive loss of R_0 and the energy left in the capacitors from the total pulse energy. After that, the energy deposition ratio ε is obtained as

$$\varepsilon = 1 - \frac{\int_0^\infty I_C^2 R_0\,\mathrm{d}t + CV_\infty^2/2}{CV_0^2/2}, \quad (4)$$

where V_∞ is the residual capacitor voltage when PSS has automatically switched off.

The results of derived parameters of all the 12 cases are compared in Fig. 11. The values are averages of three shots and the error bars show the differences between repeated shots.

Commonly, one may think that the case with higher V_0 may have higher L^* since the gas is more effectively ionized. However, in Fig. 11(b) the computed result gives a contrary conclusion. This is because under higher V_0, the plasma current sheet is more effectively accelerated and subsequently, the mutual inductance drops more rapidly. As a result, the ultimate L^* turns out to be lower. The EM coupling strength between plasma and PFN will be enhanced significantly by increasing p_0. This is because the residence time of plasma current sheet in the vicinity of drive coil is prolonged.

The increase of EM coupling strength does not lead to the increase of more energy being deposited into plasma. ε tends to drop with p_0 under higher V_0 values, while under $V_0 = 8.4$ kV, ε drops with p_0 when p_0 is small and then shifts to increase when p_0 is larger. However, the variation of ε is relatively small compared with the other two parameters. It is interesting to find that more than 77% the pulse energy is ultimately deposited into plasma in spite that L^* never exceeds 0.6.

It is reasonable to see that v_t tends to fall with the decrease of V_0 and the increase of p_0, because the total energy is larger and the accelerated mass of propellant is smaller. Although the value of L^* under $V_0 = 17.2$ kV and $p_0 = 10$ Pa is the smallest, its v_t and ε are the largest compared with other cases. The maximum v_t achieves over 1.2×10^4 m/s, which is rather competitive in in-space propulsion applications. But under $V_0 = 8.4$ kV and $p_0 \geq 50$ Pa, v_t is only several hundred m/s, even smaller than chemical rocket engines, implying that the acceleration of plasma under this condition is primarily caused by very insufficient thermal expansion.

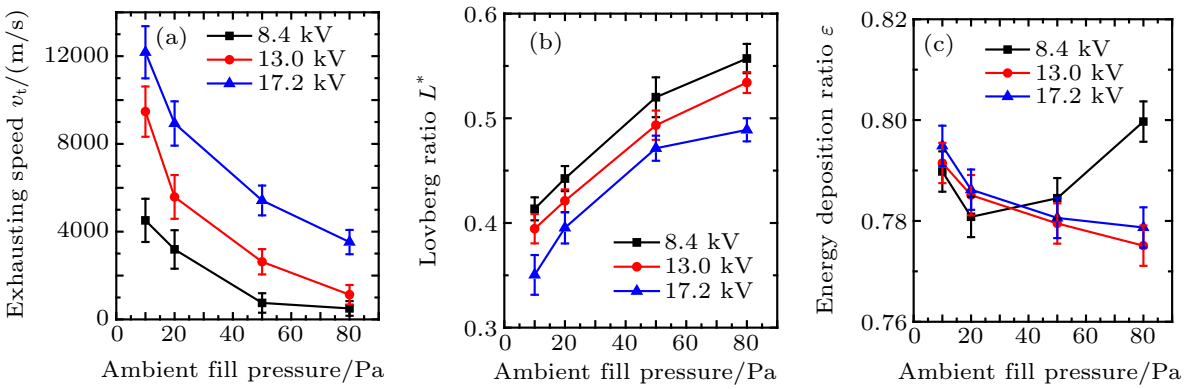


Fig. 11. Comparisons of derived parameters: (a) exhausting speed v_t, (b) Lovberg ratio L^*, (c) energy deposition ratio ε.

4. Theoretic analysis

Once a current pulse passes through drive-coil, an intense pulsed EM field is induced, which comprises an azimuthal electric field component E_θ and a radial magnetic field component B_r. E_θ breaks down the neutral gas and establishes an azimuthal current density j_θ in the plasma. Then, the axial Lorentz force generated from the interaction between j_θ and B_r compresses the plasma into a current sheet and consequently accelerates it to achieve a high speed.

4.1. Mechanism of ionization

Considering the ionization phase at the early occasion of discharge separately. It begins from the very small number of free electrons naturally existed in the neutral gas being accelerated by E_θ to collide with atoms. The resulting electron avalanche happens everywhere over the face of drive-coil. When those electron avalanches enclose to form a circular conductive channel of plasma, we say the gas breaks down. The sufficiency and immediacy of gas breakdown is the prerequisite of an effective acceleration. Different from other electric thrusters with electrodes, the initial plasma in a PIT is purely produced by spacial electron avalanche and the process is dominated by E_θ and p_0.

In accordance with Faraday's law and LCR circuit equation, the value of E_θ at $t = 0$ μs is ultimately proportional to $-V_0$,

$$E_\theta|_{t=0} \propto -\frac{\mathrm{d}\boldsymbol{B}}{\mathrm{d}t}\bigg|_{t=0} \propto -\frac{\mathrm{d}I_C}{\mathrm{d}t}\bigg|_{t=0} \propto -V_0. \tag{5}$$

We also perform a magnetic simulation using COMSOL to compute E_θ. The result indicates that, E_θ along the central line of drive-coil surface at $t = 0$ μs simply obeys $E_\theta = -0.75V_0$. The electron avalanche can be evaluated by the first Townsend's coefficient α.

$$\alpha = Ap_0 \exp\left(-\frac{B}{E_\theta/p_0}\right), \tag{6}$$

where A and B are constants determined by the range of E_θ/p_0. For the parameter range of interest in this study, α almost increases monotonically with both E_θ and p_0.[21] The magnetic field induced by drive-coil is then screened by this conductive region, whose characteristic diffusion depth δ is[14]

$$\delta = \sqrt{\frac{1}{\mu f \eta}}, \tag{7}$$

δ decreases rapidly with the plasma conductivity η, and η is well known to increase with the ionization degree of plasma.

As shown in Fig. 12(a), in the cases of higher V_0 or p_0 values (case 4 for instance), a highly conductive plasma channel is immediately established near the drive-coil face. The drive-coil field is then effectively screened and compressed by the plasma. As a result, E_θ drops sharply in the axial direction and is insufficient to ionize the gas far from the drive-coil. Meanwhile, E_θ is enhanced between the drive-coil and plasma. This positive feedback mechanism together with the compressing effect of Lorentz force results in a compact, flat, and magnetic-impermeable current sheet. The remained neutral gas far from the drive-coil is then accumulated and ionized by the current sheet when it sweeps over like a snowplow. This mode is named as the snowplow ionization mode, whose energy deposition is primarily actuated by the electric field, similar with the so-called E model in inductively coupled plasma torches.[22]

As is shown in Fig. 12(b), in the cases of lower V_0 or p_0 values (case 3 for instance), the initial breakdown may fail to produce a highly conductive plasma channel which can effectively screen the drive-coil field. E_θ then drops mildly in the axial direction and the neutral gas far from drive-coil might be ionized. Since the current density is also very ununiform in radial direction, plasma branches may emerge as is seen in Fig. 6 (#11). This ionization mode is named as the diffusive mode, whose energy deposition is primarily actuated by the magnetic field, similar with the so-called H model in inductively coupled plasma torches.[22]

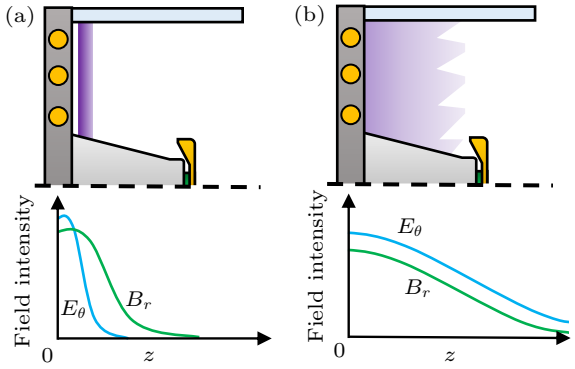


Fig. 12. Comparison of initial gas ionization mode: (a) a compact current sheet leads to snowplow ionization mode; (b) a loosen current sheet leads to diffusive ionization mode.

The snowplow mode is believed to produce higher propulsive Lorentz force since the magnetic pressure difference on the two sides of current sheet is higher under this mode.

4.2. Mechanism of acceleration

An immediate and sufficient initial ionization is the prerequisite of an efficient acceleration, but the ultimate performance is also affected by the relative time scale of current sheet movement and I_C waveform. This issue is known as the dynamic impedance matching problem.[23]

Assuming a high-quality current sheet has already been formed near drive-coil face at the beginning of discharge. Initially, the direction of drive-coil current and plasma current

is opposite and the Lorentz force is positive to push the current sheet away. As shown in Fig. 13(a), if p_0 is too large, the mass of propellant accumulated by current sheet will become so heavy that it cannot move far enough to decouple with drive-coil. Then, when I_C changes direction in the second-half period (refers to Fig. 8), the Lorentz force becomes negative and the current sheet is pulled back. This effect traps the current sheet in vicinity of drive-coil and most of the energy consumed to heat the plasma instead of accelerating it. This is what happens in case 1.

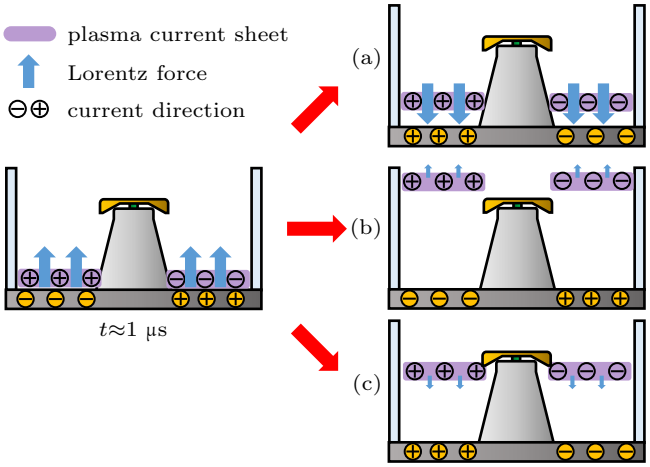


Fig. 13. Comparisons of current sheet acceleration state: (a) current sheet still resorts near drive-coil when the circuit current has already inversed; (b) current sheet has already decoupled with drive-coil before the circuit current peaks; (c) current sheet just decouples with drive-coil when circuit current inverses.

Under another circumstance as shown in Fig. 13(b), if p_0 is too small, the current sheet will move so fast that it may decouple with drive-coil too early even before I_C achieves its maximum. Then, most of the energy has not yet been released from the capacitors at that time and ultimately, it is dissipated through R_0 during the self-oscillation of PFN. However, this state is now observed in our study temporarily.

Idealistically, we want the current sheet decouples with drive-coil at the right time when I_C has just reversed as shown in Fig. 13(c), then a maximum acceleration efficiency will be achieved. This is the so-called dynamic impedance matching. However, considering the effect of secondary current sheet, the proper time occasion may shift somewhat later. The situation of case 2 to case 4 lays between Fig. 13(a) and Fig. 13(b).

The analysis above only considers the primary current sheet, besides, the effect of secondary current sheet that observed in this study should not be ignored. Some researchers have believed that the secondary current sheet may electrically short circuit the primary current sheet so that its acceleration is impaired. In some early studies, a clamping diode is employed to eliminate the I_C reversal so that the secondary current sheet might not emerge. However, the results turned out that a clamped discharge performs even worse than a ring-ring one.[22]

In fact, the so-called short circuit effect may only matter when the primary current sheet still stays in the vicinity of drive-coil after I_C passes its first zero-cross point. Once the dynamic impedance is properly matched, the emerge of secondary current sheet will no longer influence the primary one since it has already decoupled with drive-coil. Besides, because the snowplow loss of the primary current sheet is inevitable and the pulse energy is impossible to be all deposited into plasma within only one-half period. The clamped discharge is not introduced considering both propellant and energy utilization efficiency from the point of this study. From the high-speed camera photos of this study, the secondary current sheet is observed to effectively accelerate the residual propellant and soon impact into the primary current sheet. Those processes eventually make a positive contribution to the ultimate performance of a PIT.

5. Conclusion and prospect

In this study, the temporal plasma structures together with the discharge characteristics are investigated under static ambient fill condition with varied operational parameters. Based on the experimental results, the acceleration performance and plasma-circuit coupling effect are quantified. The mechanisms of both initial ionization and plasma acceleration processes are also explained.

The findings of this study indicate that both increasing p_0 and V_0 can improve the initial ionization process to produce a current sheet with higher quality. While the following acceleration process requires to meet a dynamic impedance condition. As a result, p_0 is not permitted to achieve a relative high value at present ambient fill condition. However, this conflict can be resolved by employing a pulsed gas injector. The dynamic impedance condition can be met by adjusting the gas mass bit, while p_0 can be increased by giving the puff of gas a negative speed toward the drive-coil surface.

This research helps deepen the physical understanding of PITs. The findings and conclusions derived from ambient fill tests also provide a reference for our future development of a more practical thruster equipped a pulsed gas injector. Apart from space propulsion applications, pulsed discharges are also potential in nuclear fusion studies and aircraft flow controls.[24]

References

[1] Bathgate S N, Bilek M M M and Mckenzie D R 2017 *Plasma Sci. Technol.* **19** 083001

[2] Robert H F and Ioannis G M 2005 41st *AIAA/ASME/SAE/ASEE Joint Conference and Exhibit*, July 10–13, 2005, Tucson, Arizona, USA, AIAA 2005–3892

[3] Polzin K A 2011 *J. Propul. Power* **27** 513

[4] Dailey C L and Lovberg R H 1993 *NASA Contractor Report*, Lewis Research Centre, NASA 1-19291

[5] Russell D, Poylio J H, Goldstein W, Bernard J, Lovberg R H and Dailey C L 2004 *Space* 2004 *Conference and Exhibit,* September 28–30, 2004, San Diego, California, USA, AIAA 2004-6054

[6] Choueiri E Y and Polzin K A 2006 *J. Propul. Power* **22** 611

[7] Martin A K, Dominguez A, Eskridge R H, Polzin K A and Riley D P 2015 34*th International Electric Propulsion Conference*, July 4–10, 2015, Hyogo-Kobe, Japan, IEPC 2015-50

[8] Polzin K A 2008 *IEEE Trans. Plasma Sci.* **36** 2189

[9] Dailey C L and Lovberg R H 1972 *AIAA J.* **10** 125

[10] Dailey C L and Lovberg R H 1982 *AIAA J.* **20** 971

[11] Lovberg R and Dailey C 1989 *AIAAASMESAEASEE* 25*th Joint Propulsion Conference*, July 10–12, 1989, Monterey CA, USA AIAA **89** 2266

[12] Martin A K and Eskridge R 2005 *J. Phys. D: Appl. Phys.* **38** 4168

[13] Polzin K A and Sankaran K 2013 *J. Phys. D: Appl. Phys.* **46** 5201

[14] Mikellides P G and Neilly C 2007 *J. Propul. Power* **23** 51

[15] Che B X, Li X K, Cheng M S, Guo D W and Yang X 2018 *Acta Phys. Sin.* **67** 015201 (in Chinese)

[16] Che B X, Cheng M S, Li X K and Guo D W 2018 *J. Phys. D: Appl. Phys.* **51** 365202

[17] Guo D W, Cheng M S and Li X K 2017 *Re. Sci. Instrum.* **88** 105101

[18] Yang Z, Song H M, Wang H Y, Guo S G, Jia M and Wang K 2019 *Chin. Phys. B.* **28** 024701

[19] Cheng J L, Yao X L and Sun W 2008 *Pulsed Current Technology* (Xi'an Jiaotong University Press) pp. 3–6 (in Chinese)

[20] Lovberg R H, Hayworth B R and Gooding T 1962 *Technical Report*, Convair/General Dynamics, San Diego, CA, USA, AE62-0678

[21] Wu Z C, Zhang X J and Hu Y Z 2012 *Gas Discharge* (National Defense Industry Press) pp. 66–67 (in Chinese)

[22] Guo Q J, Ni G H, Li L, Lin Q F, Zhao Y J, Sui S Y, Xie H B, Duan W X and Meng Y D 2018 *Chin. Phys. Lett.* **35** 075202

[23] Polzin K A and Choueiri E Y 2006 *IEEE Trans. Plasma Sci.* **34** 945

[24] Ji Y L, Zhou B M, Huang Y D 2018 *Chin. Phys. Lett.* **35** 055203